Bias Correction of Sentinel-2 MSI Vegetation Indices in a Desert Steppe With Original Assembled Field Online Multiangle Spectrometers

Xiaoman Fu, Yulong Bao, Bayaer Tubuxin, and Yuhai Bao

***Abstract*— In desert steppe regions with sparse vegetation, there are discrepancies between vertical and oblique observations made by satellite-based sensors. In this study, we developed and deployed an online multiangle spectrometer in the desert steppe area of Inner Mongolia, China, to calibrate satellite-based vegetation indices. One of the key components of the device is a specially designed quarter-arc iron track that holds the fixed view angles of 30°, 45°, 60°, 75°, and 90° that are fixed. These observation positions equipped with high-efficiency multichannel sensors can capture the reflectance of ground objects at visible and near-infrared wavelengths. Real-time experiments were conducted with multiple observation angles and an error-based view angle correction model was constructed to reconcile the differences between angular and vertical observations. The calculated results were subsequently applied to the bias-correction process of the Sentinel-2 vegetation index. Across all view angles, the daily distributions of the normalized difference vegetation index (NDVI) and ratio vegetation index (RVI) exhibited a U-shaped pattern with the nadir occurring at noon. Among the data, RVI demonstrated superior overall stability compared to NDVI. However, with vegetation growth, the NDVI showed less sensitivity, resulting in a decrease in its coefficient of variation (CV) from 32.3% to 18.2%. To correct the bias in Sentinel-2 products, we initially applied path length correction (PLC) to eliminate the topographic influence on the Band4 and Band8 band reflectance. Our findings revealed that Band8 performed better than Band4 in mitigating the effects of topography, as evidenced by a decrease in the determination coefficient from 0.448 to 0.09. In addition, we corrected the view angle error of the NDVI of Sentinel-2 by constructing a view angle correction model (R^2 = 0.84 and RMSE = 0.03). The corrected images exhibited significant variation characteristics in areas with relatively large view angles. The results of this study provide valuable scientific support for the correction of satellite image products and the accurate detection of vegetation through remote sensing in regions with low vegetation coverage.**

***Index Terms*— Angle correction, multiangle observation, multispectral remote sensing, normalized difference vegetation index (NDVI), ratio vegetation index (RVI).**

Manuscript received 24 March 2023; revised 19 June 2023; accepted 20 July 2023. Date of publication 15 August 2023; date of current version 29 August 2023. This work was supported in part by the Philosophy and Social Science Planning Project of Inner Mongolia Autonomous Region under Grant 2022NDA225, in part by the Key Science and Technology Project of Inner Mongolia Autonomous Region under Grant 2021ZD004503, in part by the Key Research and Development and Achievement Transformation Program of Inner Mongolia Autonomous Region under Grant 2022YFSH0070, in part by the General Program of Inner Mongolia Natural Science Foundation under Grant 2021MS04016, and in part by the Regional Program of National Natural Science Foundation of China under Grant 42261019. *(Corresponding author: Yulong Bao.)*

The authors are with the College of Geographical Science and the Inner Mongolia Key Laboratory of Remote Sensing and Geography Information System, Inner Mongolia Normal University, Hohhot 010022, China (e-mail: fxm@mails.imnu.edu.cn; baoyulong@imnu.edu.cn; tuvshin_b@imnu.edu.cn; baoyuhai@imnu.edu.cn).

Digital Object Identifier 10.1109/TGRS.2023.3305618

I. Introduction

VEGETATION plays a crucial role in the global carbon, nitrogen, and energy cycles by utilizing solar radiation through photosynthesis to convert surface elements into carbohydrates. This process, known as primary productivity, supports various organisms on Earth and influences water and material cycles [1], [2]. Grasslands and decertified lands account for a quarter of the world's land surface, with the majority consisting of sparse vegetation. Therefore, sparse vegetation can also be considered as one of the most extensive substrates on the Earth's land surface [3], [4] and is the primary vegetation cover type found in arid and semiarid regions. In these areas, where land degradation is severe, sparse vegetation serves as a key indicator of regional desertification and land degradation [5], [6]. Research conducted on desert vegetation areas has also shown that vegetation is highly sensitive to climate change [7]. Therefore, it is crucial to conduct continuous research on sparse vegetation in arid regions to enhance their recovery capacity and prevent increasingly severe catastrophic damage in the future increasingly severe catastrophic damage [8].

With the rapid development of remote sensing technology, vegetation indices have become widely used in various fields. Among them, the normalized difference vegetation index (NDVI) and the ratio vegetation index (RVI) are currently the most commonly employed indicators to characterize vegetation coverage and growth. NDVI provides an objective and effective reflection of vegetation dynamics across different spatial and temporal scales [9]. Nevertheless, the accuracy of NDVI decreases in high-density cover areas. On the other hand, RVI exhibits better accuracy in areas with higher vegetation coverage [10] and is suitable for assessing the growth and monitoring the biomass of green plants. However, vegetation spectra are influenced by various factors, such as vegetation type, coverage, and soil conditions. Changes in solar altitude angle due to different vegetation coverages affect canopy illumination and optical thickness, while variations in solar/sensor geometry impact observed data changes [11], [12]. Similarly, a shift in the sensor view angle can vary the number and composition of vegetation entering the field of view. This variation

leads to changes in the reflectance, radiation characteristics, and relative spatial distribution of ground objects, as well as some satellite products [13], [14], [15], [16], particularly in desert grassland areas with low vegetation coverage [17]. Currently, the conventional approach for obtaining vegetation indices is through calculations based on satellite image bands. Due to the differences in solar incidence angles and observation geometries during imaging caused by differences in satellite orbits, differences arise in the calculation results of different sensors [18], [19], [20]. The Sentinel-2A multispectral instrument (MSI) obtains multispectral reflectance wavelength observations with directional effects due to surface reflectance anisotropy and variations in solar and observation geometries [18]. Therefore, satellite-based vegetation index products produce different errors when monitoring vegetation, especially in the sparse vegetation of temperate desert grasslands. The correction of satellite data errors using ground data is a common method [21], [22], [23], [24]. Therefore, using field spectrometers to monitor vegetation synchronously with satellite transit, comparing the spectral characteristics of vegetation measured in the field with those of its corresponding remote sensing images, and analyzing the growth changes of vegetation reflected in the spectra through regular real measurements as a basis for correcting the spectral characteristics of remote sensing images are the important ways to reconstruct the spectral characteristics of remote sensing images and obtain accurate measurements. Aiming at the problem that scientific studies performed on this topic may yield erroneous scientific conclusions, here, we investigate systematic correction methods based on ground-truth observation experiments.

In this study, we utilized a field online multiangle spectrometer and designed and assembled by our team, to collect spectral data at various observation angles and different vegetation coverages over an extended time period (May 2021–October 2021) in the desert grassland of Siziwang Banner, Inner Mongolia, China. The objectives of the study were given as follows: 1) analyze the hourly and daily variations in NDVI and RVI with the observation of the altitude angles at different growth stages and vegetation coverages; 2) evaluate the topographic influence on the red and near-infrared reflectance of Sentinel-2 to determine whether the preprocessed L2A grade products can skip the topographic correction step in further use; and 3) construct an observation angle correction model for the vegetation indices (NDVI and RVI) to realize the systematic error correction of the Sentinel-2 satellite-based vegetation index products.

II. Data

A. Overview of the Study Site

The study was conducted in Siziwangqi (41°11′–43°23′N, 110°19′–112°59′ E), which serves a comprehensive experimental demonstration center of the Inner Mongolia Academy of Agriculture and Animal Husbandry Sciences. This area is typically regional representative of the desert grassland and agricultural–pastoral ecotones and belongs to a typical mesothermal continental monsoon climate zone, with an elevation of 1456 m. Because of the multiple pressures associated

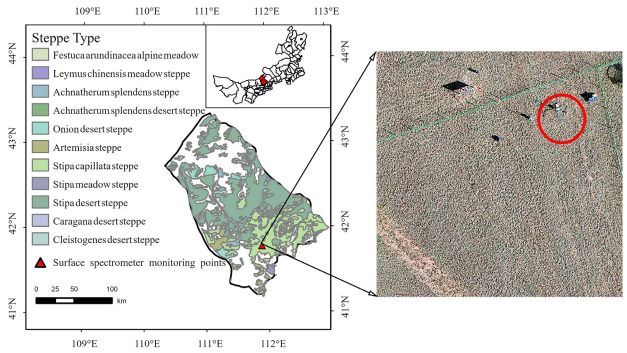

Fig. 1. Schematic of the study area.

with unreasonable exploitation, such as low precipitation, continuous drought, and long-term overgrazing, the grassland in the region has been degraded to varying degrees. The vegetation is sparse and low, with a community height of 8–10 cm and a vegetation coverage of 17%–20%. The zonal vegetation type is *Stipa breviflora* Griseb., and the main dominant species are *S. breviflora* Griseb., *Artemisia frigida*, *Neopallasia pectinata*, and *Allium tenuissimum* (Fig. 1).

B. Data Collection

The field online multiangle spectrometers analyzed herein refer to the working principle and experience of some multiangle observation equipment with a fixed field-of-view on the ground, such as the field-goniometer system (FIGOS) [25] in Switzerland, the Gonio Radiometric Spectrometer System (GRASS) [26] in U.K., and the University of Lethbridge Goniometer System (ULGS) [27] in Canada. Such instruments have the functions of automatic and real-time observations of leaf- and canopy-scale spectral data, realize the synchronous uploading of data to a platform, provide convenience for researchers to rapidly summarize and analyze data, and effectively address the problems of bulky structure, time-consuming and laborious transportation, disassembly and installation, and limited observation fields of view. These spectrometers are specifically designed to fix five observation angles of 30°, 45°, 60°, 75°, and 90° (Fig. 2). Fig. 3 shows ground photos taken from different sensor mounting angles.

Each angle is matched with a pair of two-channel light sensors (SKR 1840), which are available with a cosine-corrected diffuser or with a narrow-angle 25° field of view (Fig. 4). The wavelength range of these sensors can be set between 400 and 1050 nm with adjustable bandwidths. In a pair of sensors, one is typically equipped with a cosine-corrected diffuser, while the other has a narrow-angle field of view. The cosine error is generally less than 5% up to an angle of 60°, and absolute calibration is usually better than 5%. The sensor fit with the cosine-corrected diffuser is usually mounted with the diffuser facing upward for measuring the incident light. The purpose of this design is to monitor both incident and reflected light to eliminate the influence of fluctuating solar radiation. Moreover, a pair of sensors for collecting effective solar radiation are installed at the middle position facing upward.

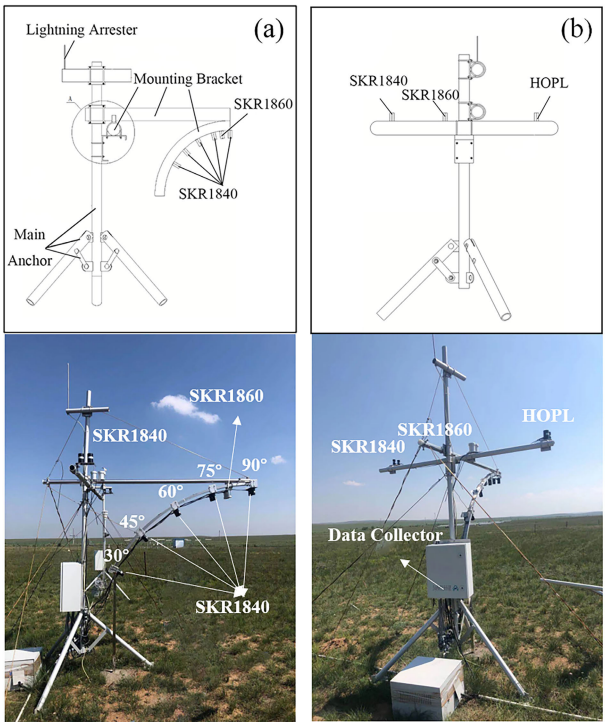

Fig. 2. Structure diagram of the field online multiangle spectrometer equipment: (a) side view and (b) back view.

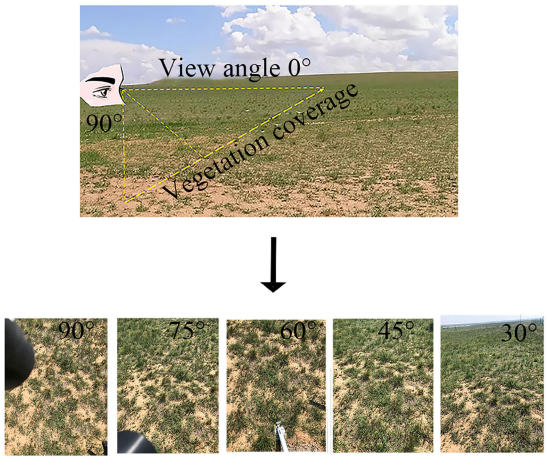

Fig. 3. (Top) Imaging of the range of views at different angles and (bottom) landscape photographs taken from different angles in the sampling area.

Fig. 4. Two-channel light sensor.

1) Field Online Spectrometer Multiangle Observation Data: Considering the vegetation growth period, which spans approximately 180 days from April to October, we focused on data from May to October 2021, covering the entire vegetation growing season. All the data were collected in real time with a time interval of 30 min. To eliminate any invalid data, we filtered out days that were affected by adverse weather conditions using the ENVIDATA-FS online system. This selection was based on a smoothed continuous effective radiation curve (9:00–15:00) and low-wind-speed dates for physiological ecological monitoring.

TABLE I
SENTINEL-2 SATELLITE-BASED VEGETATION INDEX (NDVI AND RVI) IMAGE PARAMETERS

Date	Satellite platform	Orbital number	Product level	Time	Observation angle°
210604	S2B	R118	L1C	11:15:39	8.32~11.86
210629	S2A	R118	L1C	11:15:41	8.4~11.88
210811	S2A	R018	L1C	11:25:41	1.17~8,28
210910	S2A	R018	L1C	11:25:41	1.17~8,24
211012	S2B	R118	L1C	11:16:49	8.3~11.9

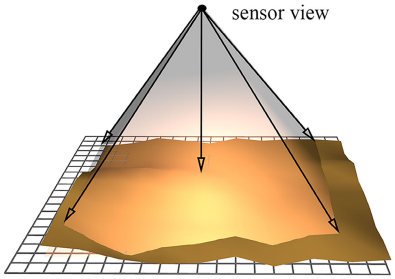

Fig. 5. Effect of topographic variations on the field-of-view observations.

2) Sentinel-2 Image Data: The Sentinel-2 satellite is part of the Copernicus Project, a collaborative initiative between the European Commission (EC) and the European Space Agency (ESA). The Sentinel-2A and 2B satellites were successfully launched on June 23, 2015, and March 7, 2017, respectively. The remote sensing image data utilized in this study were downloaded from the ESA website (URL: https://scihub.copernicus.eu/). The selected images corresponded to ground multiangle cloud-free dates and were preprocessed using the Sen2cor plug-in and SNAP software. Refer to Table I for the specific parameters of the Sentinel-2 satellite-based vegetation index (NDVI and RVI) images.

III. METHODS

A. Constructing a PLC Model for Terrain Correction

The errors in the coverage information obtained by the sensor at the subsatellite point and the edge vary depending on the change in the observation angle. In addition, topographic relief results in errors in the spectral response of nadir-pointing sensors (Fig. 5). Ratio-type vegetation indices can partially eliminate the influence of radiation variations related to the solar altitude angle, satellite observation angle, topography, cloud shadow, and other atmospheric conditions. However, complete elimination of these influences and correction for the observed zenith angle is still necessary. Furthermore, the selected band should be evaluated in terms of the mentioned factors' influence.

First, considering the influence of topographic factors, vegetation spectral features are most susceptible to both environmental elements and imaging geometry performance [28] [29].

Due to the groundward growth of vegetation, topography affects only the position of the canopy on the ground surface rather than the geometric relationship between the sun and the canopy [29]. Therefore, the topographic correction of the vegetation canopy spectra in this article is based mainly on the influence of vegetation canopy extinction paths by topographic factors. The path length correction (PLC) model is a terrain correction model because the radiation received by the sensor comes only from a single scattering from the vanes, ignoring the contribution of soil reflectivity with multiple reflections from the vanes, considering a theoretical extinction coefficient of the spherical leaf inclination angle distribution (LAD) equal to 0.5 and keeping the extinction coefficient constant for all angles by default [31]. This correction equation is expressed as follows:

$$\rho_{\mathrm{PLC}} = \rho_t \frac{S_t(\varphi_1) + S_t(\varphi_2)}{S(\varphi_1) + S(\varphi_2)} \tag{1}$$

where ρt is the vegetation canopy reflectance observed by the remote sensor, ρ_{PLC} is the vegetation canopy reflectance corrected from the slope to horizontal, $S_t(\varphi_1)$ and $S_t(\varphi_2)$ are the path lengths along the solar direction and observation direction on flat terrain, respectively, and $S(\varphi_1)$ and $S(\varphi_2)$ are the path lengths along the solar direction and observation direction on sloped terrain and path lengths on sloped terrain. Notably, (1) is corrected for terrain only, preserving the imaging geometry of the solar incidence angle and the observation angle of the remote sensor.

B. Angle Correction Equation

Then, considering the effect of the solar angle and observation angle, the influence of the solar angle refers to the difference in solar radiation received from the same surface position due to the change in the sun position and the difference in solar radiation received from different surface locations at the same moment. Among these, the solar zenith angle has a greater effect on the solar irradiance of the surface, while the variation in the solar azimuth angle usually has an effect only on the fine image features [31]. Therefore, the correction of the zenith angle is performed mainly to correct the reflectance to the solar zenith angle at local noon solar time or to the solar zenith direction angle under ground-level conditions. For the Sentinel-e remote sensing data selected in this study, the images are all taken within the period of 11:30–12:00 (Table I), and the solar zenith angle is approximately equal to the local noon solar zenith angle. In addition, the solar zenith angles of the five selected images varied in the range of [0°, 1°] and could be interpreted as the same solar irradiance at the same time, while the sunlight irradiation orientation remained unchanged, that is, the variations in the solar zenith angle and solar azimuth angle could be disregarded. Therefore, the solar zenith angle correction step was skipped in this article, and if the solar zenith angle needed to be corrected, the following correction formula was applied:

$$\mathrm{ref} = \mathrm{ref}_1/\cos\theta \tag{2}$$

where ref is the reflectance of a pixel point on a band after correction, ref_1 is the reflectance of a pixel point on a certain band before correction, and θ is the solar zenith angle.

Vegetation goes through stages of germination, flowering, and fruiting to reach senescence and death. Throughout its growth cycle, both the external phenotype and internal structure of vegetation change, leading to seasonal variations in its physiological properties and resulting in spectral characteristic changes. However, when observing the same coverage, altering the observation angle leads to variations in the proportions of vegetation and soil information entering the sensor's field of view. Therefore, it is necessary to consider the correction of the observation height angle. To address this, we converted the multiangle NDVI and RVI data selected in this article into radian data. After this step, we applied the univariate quadratic equation formula to fit the changing trend of the vegetation index on a quarter arc. The fitting formula is expressed as follows:

$$y = ax^2 + bx + c \tag{3}$$

where x represents the NDVI and RVI of the vegetation canopy collected at five different arcs y.

Subsequently, we subtracted the actual vertically downward 90° observation value from the fit multiangle value to calculate the difference between the nonvertically downward observation and downward observation of the vegetation index change. Finally, we applied different parameters for different angle changes to correct the Sentinel-2 remote sensing images using the view angle correction formula

$$\mathrm{VI}_{\mathrm{VAC}} = \mathrm{VI}_{90^\circ} - \mathrm{VI}_\theta + \mathrm{VI}_{S-2} \tag{4}$$

where $\mathrm{VI}_{\mathrm{VAC}}$ is the corrected vegetation index (NDVI, RVI), VI_{90° is the vegetation index of the actual vertical downward 90° observation, VI_θ is the predicted vegetation index under different observation angles, and VI_{S-2} is the vegetation index extracted from the Sentinel-2 remote sensing image.

We selected the coefficient of determination (R^2) to test the goodness of fit of the model and the root-mean-square error (RMSE) to check the accuracy. If the value of R^2 is larger, the NDVI and RVI fit under arc variations are better. In contrast, if the RMSE value is smaller, the fit equation predicts the data more accurately. Moreover, we chose the observation angle correction (VAC) model, which performed better between the two evaluation indicators, to improve the reliability of the correction

$$R^2 = \frac{\sum_{i=1}^{n}\left(x_i - \bar{x}\right)^2\left(y_i - \bar{y}\right)^2}{\sum_{i=1}^{n}\left(x_i - \bar{x}\right)^2\sum_{i=1}^{n}\left(y_i - \bar{y}\right)^2} \tag{5}$$

$$\mathrm{RMSE} = \sqrt{\frac{\sum_{i=1}^{n}\left(y_i - \bar{y}\right)^2}{N}}. \tag{6}$$

To evaluate the impacts of observation parameters (the time and observation angle) on the canopy VIS data more comprehensively, we also introduced the coefficient of variation (CV). The formula is shown as follows:

$$\mathrm{CV} = \frac{\frac{1}{n}\sum_{i=1}^{n}\left(x_i - \bar{x}\right)^2}{\left(x_i - \bar{x}\right)^2}. \tag{7}$$

The whole technical route used in this study is shown in Fig. 6.

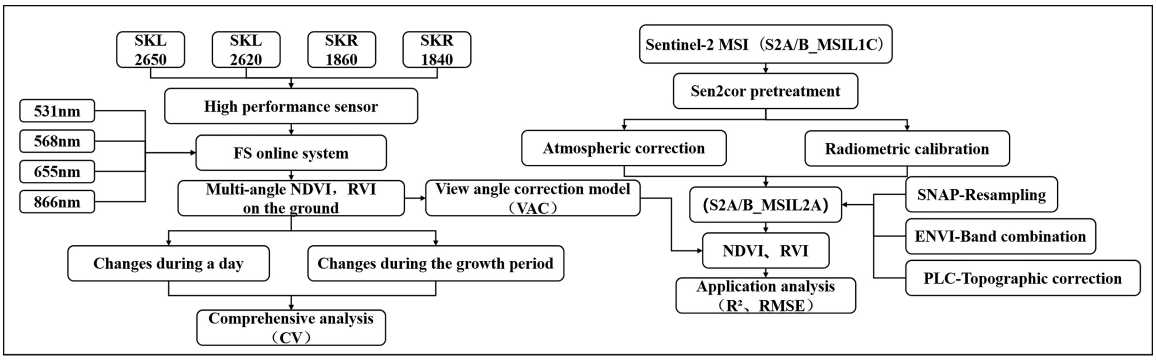

Fig. 6. Logical flowchart.

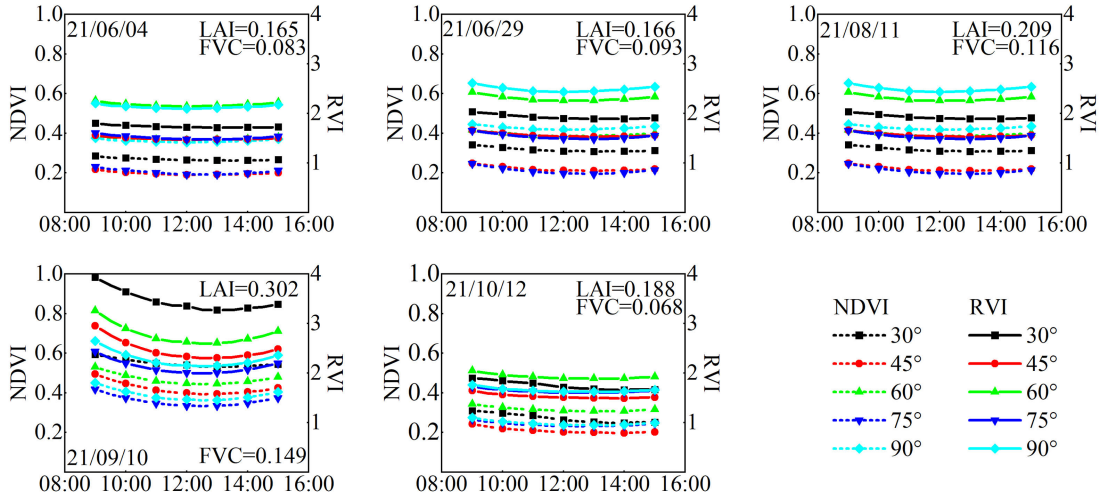

Fig. 7. Diurnal trends in the NDVI and RVI from June to October.

IV. Results and Analysis

A. Differences in Ground-Based Observation Data Under Different Angles of Observation

The hourly variation trends of NDVI and RVI, as observed through ground-based multiangle spectrometers, exhibit a similar U-shaped pattern (Fig. 7), which aligns with findings from previous studies conducted by other researchers [33].

1) Characteristics of the Hourly Scale Vegetation Index Variation: The lowest values are observed near the local noon hour, indicating a potential association with canopy photosynthesis. Chlorophyll, an essential component in the process of photosynthesis, exhibits strong absorption in the visible wavelengths and strong reflection in the near-infrared wavelengths. Around noon, as the temperature gradually rises to its peak for the day, vegetation transpiration also reaches its maximum level. In order to protect their photosynthetic organs from damage and minimize water loss, green plants reduce stomatal opening. This results in a decrease in the photosynthetic rate and, consequently, leads to lower NDVI and RVI values. Subsequently, as light and temperature gradually decrease, stomatal conductance increases, leading to an elevation in the photosynthetic rate and an increase in NDVI and RVI values.

Comparing the t and θ columns, we observe that changing the observation altitude angle has a greater impact on NDVI and RVI (Table II). Analyzing the data on a daily scale, we find that the CV of RVI due to observation angle changes is generally lower than that of NDVI, except in September. This indicates that RVI is less sensitive to variations in the observation angle compared to NDVI. Similarly, the temporal variations in RVI exhibit lower sensitivity compared to NDVI.

TABLE II
CVs of NDVI and RVI Under Different Observation Conditions

Date	LAI	FVC	NDVI (CV)		RVI (CV)	
			t	θ	t	θ
0604	0.165	0.083	5.1%	30.3%	4.5%	18.2%
0629	0.166	0.093	3.2%	32.3%	3.4%	21.8%
0811	0.209	0.116	20.3%	20.4%	4.7%	16.5%
0910	0.302	0.149	11.6%	18.9%	11.6%	21.1%
1012	0.188	0.068	8.8%	18.2%	5.1%	8.9%

2) Characteristics of Monthly Vegetation Index Changes: From the monthly scale analysis, the vegetation in the desert area at different growth stages exhibited the characteristic of sparse distribution. As the leaf area index (LAI) and fraction of vegetation cover (FVC) increase, the vegetation grows increasingly luxuriantly, causing the distance between the vegetation distribution in the observation field to shorten. Focusing on the September data shows that the NDVI is maximized (Table II). However, compared to August, the CVs of temporal variations and observation angle variations in September significantly decrease, while no such decrease is observed in RVI. This

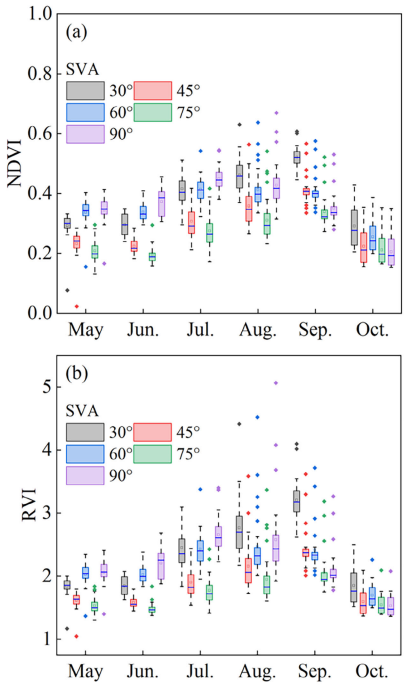

Fig. 8. Monthly scale box plots of (a) NDVI and (b) RVI from different observation angles.

suggests that as vegetation coverage increases, the sensitivity of NDVI decreases. Despite being ratio-type indices, NDVI and RVI exhibit different sensitivities to various influencing factors.

Based on the ground-based long-term data acquired by the field online multiangle spectrometer, it was observed that NDVI and RVI values follow an increasing and then decreasing trend from May to October, reaching a peak around September, which aligns with the characteristics of the vegetation growth cycle. Comparing the graphs in Fig. 8, it is evident that NDVI values at different observation angles exhibit varying aggregations in different months. The aggregation phenomenon is more pronounced for RVI compared to NDVI. This further confirms that RVI is less sensitive to changes in the viewing angle than NDVI. In addition, when analyzing the multiangle data, it is observed that with more lush vegetation growth, the overall values of the two vegetation indices under oblique observation conditions (i.e., 30° observations) surpass those of the other four angles in August and September.

The tilt angle increases the amount of vegetation entering the field of view. Vegetation in the observed area, being 3-D and having a certain height, becomes more visible when the observation angle is tilted. Consequently, the vegetation index appears higher compared to the actual value obtained from vertical downward observations. In September, when vegetation coverage is at its highest, the multiangle observations of both indices consistently reflect this characteristic.

The observed angular variation CVs for NDVI vary from 6.7% to 25.8%, and the observed angular variation CVs for RVI range from 5.2% to 25.2% (Table III). Notably, the CV of observed angular variations in RVI is higher at 30° and 60° in mid-July, at 30°, 60°, and 90° in mid-August, and at 30°, 45°, and 60° in mid-September compared to the corresponding angles for NDVI in the respective months. This suggests that RVI exhibits lower angular sensitivity than NDVI for most of the study period. However, when vegetation experiences rapid growth, the tilt angle can have a greater effect on RVI. Nevertheless, this effect is minimal when considering vertical or inclined observations.

B. Analysis of Terrain Correction Results

We extracted the solar zenith angle and solar azimuth angle at the instant of the Sentinel-2 satellite image that was acquired using ESA-SNAP software. As shown in Fig. 9, the solar zenith angle varies by approximately 1° in the same image, and the solar zenith angle gradually increases from the bottom-right to the top-left corner. The variation in the solar azimuth is approximately 8° in the same image, and the direction of the variation is not consistent with the solar zenith angle, which gradually increases from the bottom-left to the top-right corner.

Our analysis of the influence of sun angle changes on surface radiation indicates that variations in the sun zenith angle have a greater impact on the solar irradiance of the surface, while changes in the sun azimuth angle primarily affect image detail features. Therefore, considering that the image acquisition times of the remote sensing data selected in this experiment were between 11:30 and 12:00 (Table I) and the solar zenith angle variations were all in the range of [0°, 1°] (Fig. 9) with a small degree of variation, we can approximate the solar zenith angle at the moment of acquisition of the remote sensing data used in this experiment as being equal to the local noon solar zenith angle. Consequently, at the time of acquisition, the solar irradiance remains the same, and the orientation of sunlight irradiation remains unchanged, without considering the variations in solar zenith and azimuth angles.

In this experiment, we used ESA-SNAP software to extract the observation angles of the remote sensing image on September 10, 2021, and found that the observation altitude angles as well as the observation azimuth angles recorded in two bands, Band4 and Band8, within the same image element of the same image scene were different, as shown in Figs. 10 and 11. To improve the accuracy of the whole experimental process, we chose Band4 and Band8 to be processed separately in the process of PLC topographic correction of remote sensing images. Since the B4 and B8 bands correspond to the green and near-infrared bands, respectively, and respond differently to the terrain, performing separate topographic correction is necessary to improve the accuracy of the processed data.

The reflectivity data of different slope changes shown in Fig. 12 reflected two sets of local areas with varying slope variations derived from remote sensing images taken on the same day by the Sentinel-2 satellite. One of the groups was a flat area in the slope variation range of 2°–5°, and the other was an undulating area in the field of 10°–20° slope variations. The flat areas were in the 2 × 2 km range centered on the multiangle observation experiment site. Uncorrected density scatter plots and density scatter plots after PLC terrain correction were drawn for the two datasets. The figure was plotted with the cos value of the angle between the solar

TABLE III
CV OF NDVI AND RVI FROM DIFFERENT OBSERVATION ANGLES

Month	NDVI (CV)					RVI (CV)				
	30°	45°	60°	75°	90°	30°	45°	60°	75°	90°
5	15.2%	19.2%	12.6%	18.4%	12.1%	8.1%	8.1%	8.4%	8.3%	8.4%
6	12.1%	10.9%	7.6%	13.7%	11.6%	7.9%	5.2%	6.0%	6.0%	10.0%
7	12.4%	16.4%	9.9%	18.5%	8.4%	12.9%	11.6%	10.7%	11.9%	10.2%
8	12.2%	18.5%	16.3%	24.2%	18.4%	16.2%	17.8%	21.0%	20.7%	25.2%
9	6.7%	11.3%	12.1%	16.2%	15.2%	10.0%	13.3%	14.7%	15.3%	15.0%
10	23.3%	25.8%	19.1%	21.5%	24.0%	15.7%	12.7%	12.7%	10.2%	11.0%

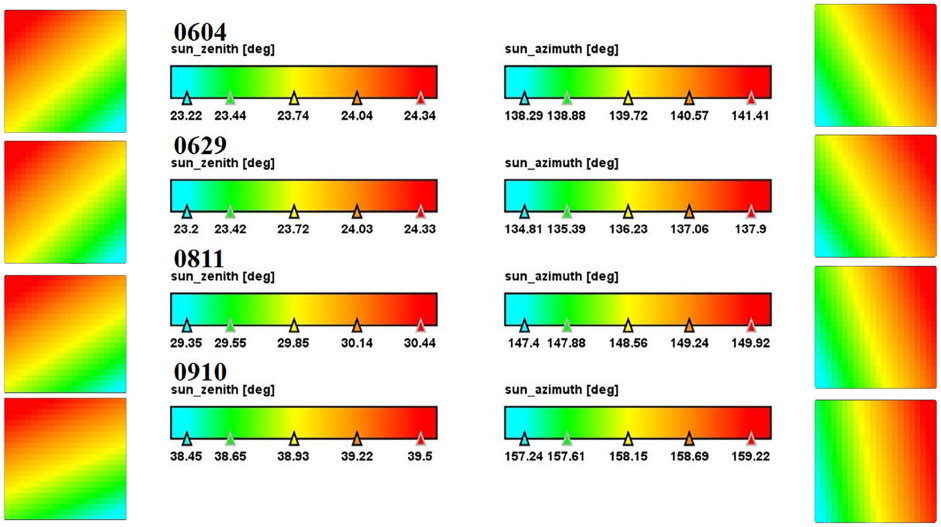

Fig. 9. Sentinel-2 remote sensing image solar zenith angle and solar azimuth angle.

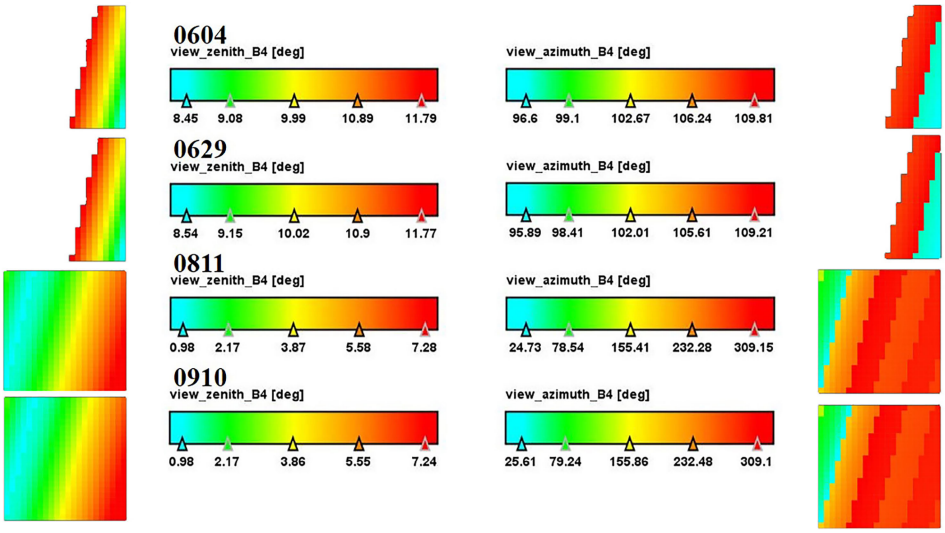

Fig. 10. Sentinel-2 remote sensing image Band4 view zenith angle and view azimuth angle.

incidence and the local normal as the horizontal coordinate and the reflectance in the red and near-infrared bands as the vertical coordinate. The results show that the red and near-infrared band reflectances in the area with small slope changes did not correlate with cos(i), so the PLC model correction could be omitted. The correction was obvious for slope changes between 10° and 20° (Fig. 12 and Table IV). Both the red and near-infrared band reflectances before correction were significantly positively correlated with cos(i). After the PLC model treatment, R^2 was reduced considerably, indicating that the terrain effect was attenuated. Moreover, the R^2 value of the uncorrected NIR band was greater than that of the red band, while the R^2 value of the corrected NIR band was smaller than that of the red band except on September 10, 2021. The above results indicate that the effect of topographic changes on the NIR band was greater than that on the red band, and

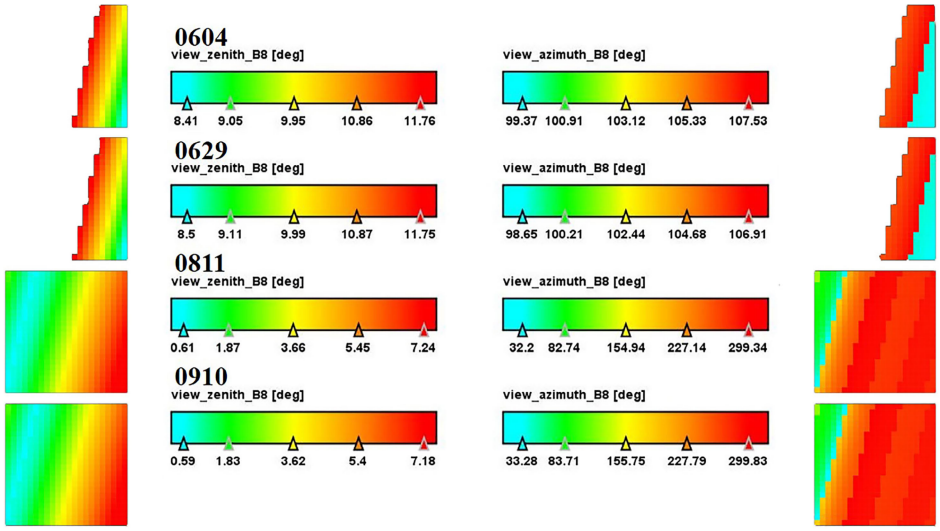

Fig. 11. Sentinel-2 remote sensing image Band8 view zenith angle and view azimuth angle.

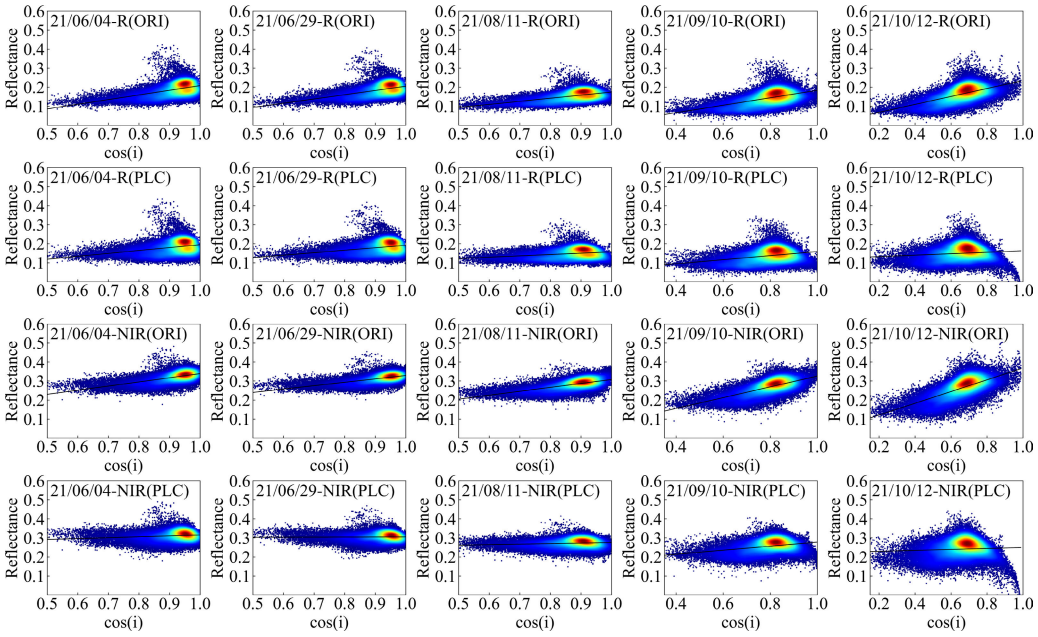

Fig. 12. Density scatterplots between the Band4 and Band8 band reflectances and the cosine of the local solar incidence angle [cos(i)] before (ORI) and after (PLC) topographic correction.

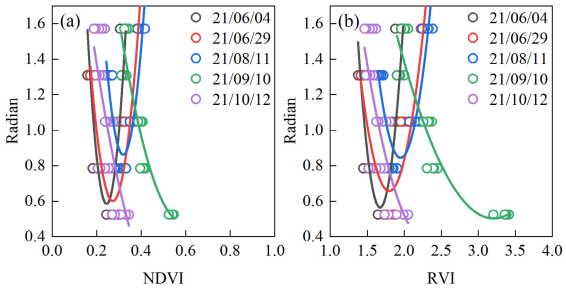

Fig. 13. Fitting curves of the variations in (a) NDVI and (b) RVI in one-quarter arc.

the correction effect of the NIR band using the PLC model was greater than that of the red band.

C. Analysis of Observation Angle Correction Results

After fitting the trend to the radian changes in NDVI and RVI (Fig. 13 and Tables V and VI), it was observed that the fit-equation R^2 value for each date was greater than 0.5, with the highest value reaching 0.85. The RMSE value was calculated between the predicted values obtained from the fit equations and the true values derived from the multiangle NDVI and RVI data collected on that date. The final result revealed that the RMSE was very small, indicating that the error between the predicted and true values obtained by the fit equations was small, and the equations could thus predict multiangle observations more accurately. Therefore, these data could be reliably used in the subsequent calibration steps.

Using the Sentinel-2 NDVI image taken on September 10, 2021, as an example, the VAC observation model was used for correction (Fig. 14). Fig. 14(a) shows an uncorrected NDVI remote sensing image of the study area, while Fig. 14(b) shows the corrected NDVI remote sensing image of the study area. The solid boxes in the two figures show the areas with less variation in the zenith angle of the observa-

TABLE IV

REGRESSION OF THE BAND4/BAND8 RESULTS BETWEEN THE REFLECTANCE (y) AND THE COSINE OF THE LOCAL SOLAR INCIDENCE ANGLE (x). RELATIVELY LOW SLOPE AND R^2 VALUES OF THE FIT LINE INDICATE A BETTER CORRECTED RESULT. RF REPRESENTS THE REGRESSION FUNCTION

Date	Red band (Original)		Red band (PLC)		Near-infrared band (Original)		Near-infrared band (PLC)	
	RF	R^2	RF	R^2	RF	R^2	RF	R^2
0604	y = 0.245x - 0.037	0.244	y = 0.153x + 0.042	0.1	y = 0.218x + 0.121	0.312	y = 0.046x + 0.269	0.016
0629	y = 0.223x - 0.019	0.249	y = 0.129x + 0.062	0.088	y = 0.178x + 0.151	0.297	y = 0.0036x + 0.301	0.0001
0811	y = 0.162x + 0.012	0.242	y = 0.07x + 0.087	0.05	y = 0.206x + 0.101	0.351	y = 0.027x + 0.248	0.009
0910	y = 0.196x - 0.013	0.254	y = 0.107x + 0.052	0.085	y = 0.283x + 0.042	0.448	y = 0.1068x + 0.171	0.09
1012	y = 0.209x + 0.026	0.330	y = 0.038x + 0.125	0.013	y = 0.309x + 0.059	0.447	y = 0.025x + 0.224	0.004

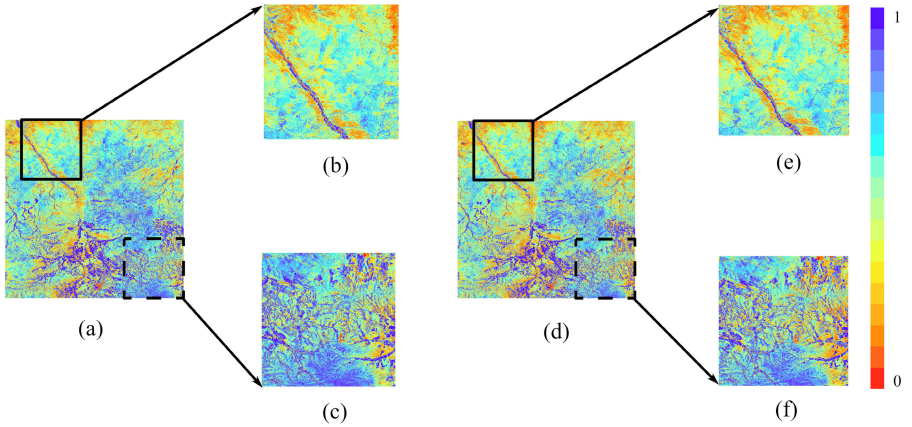

Fig. 14. (a) NDVI images before and (d) after elevation angle correction. (b) and (e) Range of the solid line frame is the area with a small change in the viewing angle and (c) and (f) range of the dashed line frame is the area with a large change in the viewing angle.

TABLE V

FITTING POLYNOMIAL, R^2, AND RMSE VALUES (NDVI)

Date	NDVI		
	RF	R^2	RMSE
0604	Y=-64.94x+132.85x^2+8.52	0.62	0.01
0629	Y=-40.64x+74.52x^2+6.14	0.83	0.012
0811	Y=-58.76x+92.14x^2+10.23	0.65	0.02
0921	Y=-16.28x+13.87x2+5.26	0.84	0.03
1012	Y=-12.5x+11.4x2+3.42	0.503	0.03

TABLE VI

FITTING POLYNOMIAL, R^2, AND RMSE VALUES (RVI)

Date	RVI		
	RF	R^2	RMSE
0604	Y=-35.3x+10.54x^2+30.112	0.71	0.03
0629	Y=-15.32x+4.26x^2+14.42	0.79	0.07
0811	Y=-20.25x+5.19x^2+20.59	0.75	0.05
0921	Y=-3.88x+0.61x^2+6.72	0.85	0.14
1012	Y=-7.09x+1.54x^2+8.55	0.50	0.10

tions, corresponding to the zoomed-in local images shown in Fig. 14(b) and (e). The dashed boxes show the area with relatively high zenith angle variations in this image, corresponding to the local zoom images shown in Fig. 14(c) and (f). Comparing Fig. 14(c) and (f), the difference in this region ranges from [0, 0.019], and the average difference is 0.015. Therefore, there is a significant color change after VAC correction. Comparing Fig. 14(b) and (e), the difference in this region ranges from [0, 0.005] with a mean difference of 0.004. Therefore, there is no significant color change after VAC correction. These findings indicate that the model exhibited better correction performance in areas with substantial changes in the viewing angle [Fig. 14(c) and (f)], while the impact on areas with small angle variations was negligible.

V. CONCLUSION

Our study has significant implications for monitoring the vast grasslands in the desert steppe region. Through near-surface multiangle observation experiments using the originally designed field online multiangle spectrometer, we have drawn the following conclusions.

1) The daily NDVI and RVI curves exhibited similar U-shaped trends, with the lowest values occurring near local noon. RVI was found to be less sensitive to changes in the viewing angle compared to NDVI. However, the sensitivity of NDVI decreased as vegetation became lusher. In sparse vegetation areas, such as the one studied in this article, larger observation angles resulted in greater errors in the vegetation index. This outcome may be related to photosynthesis in plants. Chlorophyll, an important pigment for photosynthesis, undergoes a "lunch break" phenomenon at noon in the grass herbage of desert steppe. Therefore, changes in NDVI and RVI over time are also related to photosynthesis. Factors, such as leaf stomatal opening, light intensity,

temperature, water, and CO_2 concentration, affect vegetation photosynthesis. When the midday solar irradiation intensity exceeds the threshold required for plant photosynthesis, and with increasing temperature enhancing vegetation transpiration, the photosynthetic rate of leaves decreases to prevent damage to photosynthetic organs and excessive water loss from cells. As stomatal opening decreases, the photosynthetic rate also decreases, leading to a decline in NDVI and RVI values. With the gradual decrease in light and temperature, stomatal conductance increases, resulting in an increase in the photosynthesis rate and subsequent elevation of NDVI and RVI values.

2) Our results indicate that Sentinel-2 L2A data with slope variations in the range of 10°–20° require topographic correction to eliminate reflectance differences caused by topographic factors. We applied the PLC model and observed that the NIR band's intensity was slightly higher than that of the red band before correction, with the NIR band performing better after correction. The determination coefficient (R^2) decreased from 0.448 to 0.09, primarily due to the longer wavelength of the near-infrared band, which falls between visible light and infrared light. This longer wavelength enables the near-infrared band to penetrate various occlusions such as the atmosphere, surface, and vegetation, making it more susceptible to topographic effects. In addition, the near-infrared band's infrared component is absorbed by vegetation and other surface covers, while the red band reflected by the surface is mainly concentrated in the visible light range. Consequently, the near-infrared band is more dependent on the reflection and transmission of vegetation when reflecting surface characteristics. The variation in vegetation type in regions with complex terrain can lead to significant changes in the near-infrared band's reflection intensity in remote sensing images. These factors make the near-infrared band more susceptible to terrain effects compared to the red band.

3) We developed fitting equations based on the observed angular variation patterns of NDVI and RVI. Our results indicate that the estimation model performed best on September 10, with a coefficient of determination of 0.84 and an RMSE of 0.03 for NDVI, as well as R^2 and RMSE values of 0.85 and 0.14 for RVI, respectively. These findings demonstrate that the multiangle estimation model established for monitoring NDVI and RVI vegetation indices using a ground-based multiangle spectrometer exhibited good estimation accuracy. The model can be used to correct errors in the Sentinel-2 vegetation index, especially in areas with significant observation angle changes.

In this article, an angle correction model was constructed using vegetation indices measured by a ground-based multiangle spectrometer. The model was implemented to correct the Sentinel 2 product enhancing their accuracy and reliability. By calculating vegetation indices for different viewing angles based on measured multiangle spectral data, we were able to accurately restore the apparent reflectance of Sentinel-2 products, eliminating the influence of atmospheric interference, soil background, and terrain effects on vegetation indices. Consequently, more reliable vegetation information can be obtained. However, there are still some limitations of the vegetation index measured by using ground-based multiangle spectrometer. Extending ground-based data to satellite data cannot completely eliminate spatial mismatch, which may lead to subtle biases in the quality of satellite calibration data as well as not considering the influence of the spectral response function by Sentinel-2 in this study. Therefore, we believe that it is important for future research to understand and quantify the potential impacts of such mismatches. In addition, our online multiangle spectrometer is a fixed field-of-view device that cannot be moved. It only observes canopy reflections in the forward scattering region, and the resulting data are relatively homogeneous. Once the vegetation in the study area is destroyed, large errors may arise, resulting in unusable data for the entire experimental period. Therefore, in the subsequent research, we will work on improving the online equipment that can achieve all-round observation. It is planned to fix the hyperspectral imager used on the UAV on an omnidirectional mount to obtain full-angle (altitude angle and azimuth angle) hyperspectral image data. To achieve more accurate, full-angle, continuous-time sampling observations of different grassland types.

REFERENCES

[1] M. Peter, "Energy production from biomass (Part 1): Overview of biomass," *Bioresource Technol.*, vol. 83, no. 1, pp. 37–46, May 2002.

[2] V. Smil, "Global material cycles and energy," in *Encyclopedia of Energy*, New York, NY, USA: Elsevier, vol. 3, 2004, pp. 23–32.

[3] Y. Hu, S. Sun, and Y. Zheng, "Review of study on interaction between underlying surface with sparse vegetation and atmosphere," *Plateau Meteorol.*, vol. 23, no. 3, pp. 281–296, 2004.

[4] L. Jiang, A. Bao, H. Guo, and F. Ndayisaba, "Vegetation dynamics and responses to climate change and human activities in central Asia," *Sci. Total Environ.*, vols. 599–600, pp. 967–980, Dec. 2017.

[5] U. Gessner, V. Naeimi, I. Klein, C. Kuenzer, D. Klein, and S. Dech, "The relationship between precipitation anomalies and satellite-derived vegetation activity in central Asia," *Global Planet. Change*, vol. 110, pp. 74–87, Nov. 2013.

[6] J. Yao, Z. Liu, and Q. Yang, "Temperature variability and its possible causes in the typical basins of the arid central Asia in recent 130 years," *Acta Geographica Sinica*, vol. 69, no. 3, pp. 291–302, Mar. 2014.

[7] M. Berdugo et al., "Global ecosystem thresholds driven by aridity," *Science*, vol. 367, no. 6479, pp. 787–790, Feb. 2020.

[8] Y. Peng et al., "Global dryland ecosystem programme (G-DEP): Africa consultative meeting report," *J. Arid Land*, vol. 12, no. 3, pp. 538–544, May 2020.

[9] K. Jin, F. Wang, and J. Han, "Contribution of climatic change and human activities to vegetation NDVI change over China during 1982–2015," *Acta Geographica Sinica*, vol. 75, no. 5, pp. 961–974, May 2020.

[10] G. Gao and S. Wang, "Compare analysis of vegetation cover change in Jianyang city based on RVI and NDVI," in *Proc. 2nd Int. Conf. Remote Sens., Environ. Transp. Eng.*, Jun. 2012, pp. 1–4.

[11] J. N. Epiphanio and A. R. Huete, "Dependence of NDVI and SAVI on sun/sensor geometry and its effect on fAPAR relationships in Alfalfa," *Remote Sens. Environ.*, vol. 51, no. 3, pp. 351–360, Mar. 1995.

[12] C. Coll, J. M. Galve, and R. Niclòs, "Angular variations of brightness surface temperatures derived from dual-view measurements of the advanced along-track scanning radiometer using a new single band atmospheric correction method," *Remote Sens. Environ.*, vol. 223, pp. 274–290, Jan. 2019.

[13] D. S. Kimes, "Remote sensing of temperature profiles in vegetation canopies using multiple view angles and inversion techniques," *IEEE Trans. Geosci. Remote Sens.*, vol. GE-19, no. 2, pp. 85–90, Apr. 1981.

[14] W. Qin and Y. Xiang, "Influence of vegetation structure and sun/view geometry on NDVI," *Remote Sens. Environ. China*, vol. 11, no. 4, pp. 285–290, 1996.
[15] X. Zhang, Q. Tian, and R. Shen, "Analysis of directional characteristics of winter wheat canopy spectra," *Spectrosc. Spectral Anal.*, vol. 30, no. 6, pp. 1600–1605, Jun. 2010.
[16] S. L. Ermida, I. F. Trigo, C. C. DaCamara, F. M. Göttsche, F. S. Olesen, and G. Hulley, "Validation of remotely sensed surface temperature over an oak woodland landscape—The problem of viewing and illumination geometries," *Remote Sens. Environ.*, vol. 148, pp. 16–27, May 2014.
[17] J. R. Norris and J. J. Walker, "Solar and sensor geometry, not vegetation response, drive satellite NDVI phenology in widespread ecosystems of the western United States," *Remote Sens. Environ.*, vol. 249, Nov. 2020, Art. no. 112013.
[18] D. P. Roy, J. Li, H. K. Zhang, L. Yan, H. Huang, and Z. Li, "Examination of sentinel-2A multi-spectral instrument (MSI) reflectance anisotropy and the suitability of a general method to normalize MSI reflectance to nadir BRDF adjusted reflectance," *Remote Sens. Environ.*, vol. 199, pp. 25–38, Sep. 2017.
[19] F. Gao, M. C. Anderson, W. P. Kustas, and R. Houborg, "Retrieving leaf area index from Landsat using MODIS LAI products and field measurements," *IEEE Geosci. Remote Sens. Lett.*, vol. 11, no. 4, pp. 773–777, Apr. 2014.
[20] B. Qin et al., "A thermal radiation directionality correction method for the surface upward longwave radiation of geostationary satellite based on a time-evolving kernel-driven model," *Remote Sens. Environ.*, vol. 294, Aug. 2023, Art. no. 113599.
[21] H. Reese and H. Olsson, "C-correction of optical satellite data over Alpine vegetation areas: A comparison of sampling strategies for determining the empirical c-parameter," *Remote Sens. Environ.*, vol. 115, no. 6, pp. 1387–1400, Jun. 2011.
[22] W. Abera, L. Brocca, and R. Rigon, "Comparative evaluation of different satellite rainfall estimation products and bias correction in the Upper Blue Nile (UBN) basin," *Atmos. Res.*, vols. 178–179, pp. 471–483, Sep. 2016.
[23] L. Zhou et al., "A study on availability of ground observations and its impacts on bias correction of satellite precipitation products and hydrologic simulation efficiency," *J. Hydrol.*, vol. 610, Jul. 2022, Art. no. 127595.
[24] Z. Shen and H. Wu, "A comparative analysis of merging strategies for satellite precipitation estimates and ground observations over Chinese mainland," *J. Atmos. Solar-Terr. Phys.*, vol. 246, May 2023, Art. no. 106072.
[25] S. R. Sandmeier and K. I. Itten, "A field goniometer system (FIGOS) for acquisition of hyperspectral BRDF data," *IEEE Trans. Geosci. Remote Sens.*, vol. 37, no. 2, pp. 978–986, Mar. 1999.
[26] H. Pegrum, N. Fox, M. Chapman, and E. Milton, "Design and testing a new instrument to measure the angular reflectance of terrestrial surfaces," in *Proc. IEEE Int. Symp. Geosci. Remote Sens.*, Denver, CO, USA, Jul. 2006, pp. 1–6.
[27] C. A. Coburn and D. R. Peddle, "A low-cost field and laboratory goniometer system for estimating hyperspectral bidirectional reflectance," *Can. J. Remote Sens.*, vol. 32, no. 3, pp. 244–253, Jan. 2006.
[28] X. Yang, X. Zuo, W. Xie, Y. Li, S. Guo, and H. Zhang, "A correction method of NDVI topographic shadow effect for rugged terrain," *IEEE J. Sel. Topics Appl. Earth Observ. Remote Sens.*, vol. 15, pp. 8456–8472, 2022.
[29] H. Jin, A. Li, W. Xu, Z. Xiao, J. Jiang, and H. Xue, "Evaluation of topographic effects on multiscale leaf area index estimation using remotely sensed observations from multiple sensors," *ISPRS J. Photogramm. Remote Sens.*, vol. 154, pp. 176–188, Aug. 2019.
[30] J. Wen, Q. Liu, and Q. Xiao, "Assessment of different topographic correction methods and validation," *J. Beijing Normal Univ., Natural Sci.*, vol. 43, no. 3, pp. 255–263, 2007.
[31] G. Yin et al., "PLC: A simple and semi-physical topographic correction method for vegetation canopies based on path length correction," *Remote Sens. Environ.*, vol. 215, pp. 184–198, Sep. 2018.
[32] L. Li, Y. Hu, and C. Gong, "Solar elevation angel's effect on image energy and its correction," *J. Atmos. Environ. Opt.*, vol. 8, no. 1, pp. 11–17, Jan. 2013.
[33] R. Fensholt, I. Sandholt, S. Stisen, and C. Tucker, "Analysing NDVI for the African continent using the geostationary Meteosat Second Generation SEVIRI sensor," *Remote Sens. Environ.*, vol. 101, no. 2, pp. 212–229, Mar. 2006.

Xiaoman Fu received the M.Sc. degree in geography from Inner Mongolia Normal University, Hohhot, China, in 2023.

Her research interests include multiangle imaging spectroscopy in vegetation canopies.

Yulong Bao received the Ph.D. degree in environmental planning and management from Northeast Normal University, Changchun, China, in 2013.

He visited Nagoya University, Nagoya, Japan, from July 2017 to July 2018, to study abroad. From September 2013 to December 2018, he worked as a Lecturer at the College of Geographical Science, Inner Mongolia Normal University, Hohhot, China. In December 2018, he worked as an Associate Professor at the College of Geographical Science, Inner Mongolia Normal University. His work focuses on disaster and environmental risk-related research, including forest grassland fire, black and white disaster, rat damage, and grassland degradation spatial scale effect mechanism.

Bayaer Tubuxin received the M.S. degree from the Department of Environmental Science on Biosphere, Graduate School of Agriculture, Tokyo University of Agriculture and Technology, Tokyo, Japan, in 2011, and the Ph.D. degree in biological and environmental engineering from the Graduate School of Agriculture and Life Sciences, University of Tokyo, Tokyo, in 2016.

Since January 2019, he has been working as a Lecturer at the College of Geographical Science, Inner Mongolia Normal University, Hohhot, China. His work focuses on vegetation change and response mechanism of climate elements and physiological and ecological characteristics of typical plants in desert steppe of Mongolian Plateau.

Yuhai Bao received the Ph.D. degree in cartography and geography information system from the Institute of Remote Sensing Applications, Chinese Academy of Sciences, Beijing, China, in 1999.

In September 2016, he was the Dean of the College of Geographical Science, Inner Mongolia Normal University, Hohhot, China. For many years, he has been engaged in the research on resource and environment investigation, comprehensive application of 3S technology, and natural disaster risk assessment and early warning on the Mongolian Plateau, has a more comprehensive understanding of the resource environment and natural disaster situation on the Mongolian Plateau, and has accumulated a large amount of basic data and first-hand investigation information.